

# Continuum Strong Discontinuity Approach to fracture of concrete

J. Oliver, A.E. Huespe, M.D.G. Pulido & S. Blanco

Technical University of Catalonia (UPC), Campus Nord UPC, Mòdul C-1  
Jordi Girona 1-3, 08034 Barcelona, Spain

**ABSTRACT:** The paper presents the essentials of the Continuum Strong Discontinuity Approach to fracture mechanics (CSDA) applied to fracture of concrete. After a brief description of the main ingredients of the CSDA, the methodology is applied to the numerical simulation of several problems of fracture in concrete, including multiple fractures in reinforced concrete, and 2D and 3D simulations.

**Keywords:** strong discontinuities, fracture, concrete, failure, numerical simulation

## 1 MOTIVATION: CONTINUUM FAILURE AND DISCONTINUITIES

Failure of concrete is characterized by the appearance of macroscopic displacement discontinuities that we commonly term cracks. The onset and development of these cracks does not take place suddenly but they appear gradually as the coalescence of micro-cracks due to small-scale dissipation mechanisms.

Therefore, from the physical point of view there is a transition, as deformation takes place at a given material point, between the continuum regime and the appearance of dissipative cracks displaying discontinuous displacements (see Figure 1). The locus of material points experiencing that transition, is commonly termed in fracture mechanics the *Fracture Process Zone* (Bažant and Planas 1998).

On those physical grounds, one could think that those non-linear *continuum* (stress-strain) constitutive models, commonly used in continuum approaches to concrete failure, and the *discrete laws* (traction-separation laws), considered in non-linear fracture mechanics, are not independent from each other. Indeed, when successful in modeling failure of concrete, both types of constitutive models must be intimately related.

This work deals on this topic. In next sections it is first sketched the so-called Continuum Strong Discontinuity Approach (CSDA) whose fundamentals have been presented in detail

elsewhere (see Oliver et al. (1999), Oliver (2000), Oliver et al. (2001)). Then, applications to simulations of fracture of concrete are presented and the conclusions of the work are outlined.

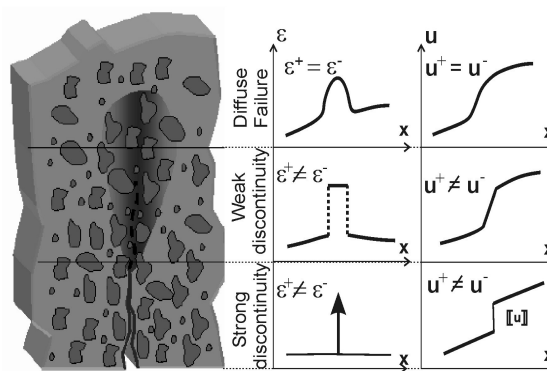


Figure 1: Kinematics in the fracture process zone

## 2 A CONTINUUM STRONG DISCONTINUITY APPROACH (CSDA) TO FRACTURE

The CSDA aims at bridging continuum mechanics and non-linear fracture mechanics, in such a way that: a) both the continuum and discrete failure mechanisms can be modeled and captured using a common continuum format and, b) the transition between both regimes is naturally recovered. The

main ingredients of the approach are sketched in next sections.

### 2.1 Kinematics

An admissible displacement field  $\mathbf{u}(\mathbf{x})$ , exhibiting displacement discontinuities, see Figure 2, can be described by:

$$\mathbf{u}(\mathbf{x}) = \bar{\mathbf{u}}(\mathbf{x}) + \mathcal{H}_S[[\mathbf{u}]](\mathbf{x})$$

$$\mathcal{H}_S = \begin{cases} = 1 \quad \forall \mathbf{x} \in \Omega^+ \\ = 0 \quad \forall \mathbf{x} \in \Omega^- \end{cases} \quad (1)$$

where  $\bar{\mathbf{u}}$  is a smooth field and  $\mathcal{H}_S[[\mathbf{u}]](\mathbf{x})$  ( $\mathcal{H}_S$  being the Heaviside/step function shifted to  $S$ ) captures the displacement jump field  $[[\mathbf{u}]](\mathbf{x})$  at the discontinuity interface  $S$  of normal  $\mathbf{n}$ , which divides the body  $\Omega$  into two disjoint parts  $\Omega^+$  and  $\Omega^-$ .

The strain field kinematically compatible with the discontinuous displacement field (1) is then:

$$\boldsymbol{\varepsilon}(\mathbf{x}) = \nabla^S \mathbf{u}(\mathbf{x}) = \underbrace{\bar{\boldsymbol{\varepsilon}}(\mathbf{x})}_{\text{regular (bounded)}} + \underbrace{\delta_S([[ \mathbf{u} ]]) \otimes \mathbf{n}}_{\text{singular (unbounded)}} \quad (2)$$

which displays an unbounded term due to the presence of the Dirac's delta function  $\delta_S$ . For computational purposes, the singular term in equation (2) should be regularized through the following "h-sequence" in terms of the bandwidth  $h$  of the regularization domain  $S^h$  (see Figure 2):

$$\delta_S(\mathbf{x}) = \lim_{h \rightarrow 0} \frac{\mu_S}{h} \quad ; \quad \mu_S(\mathbf{x}) = \begin{cases} = 1 \quad \forall \mathbf{x} \in S^h \\ = 0 \quad \text{otherwise} \end{cases} \quad (3)$$

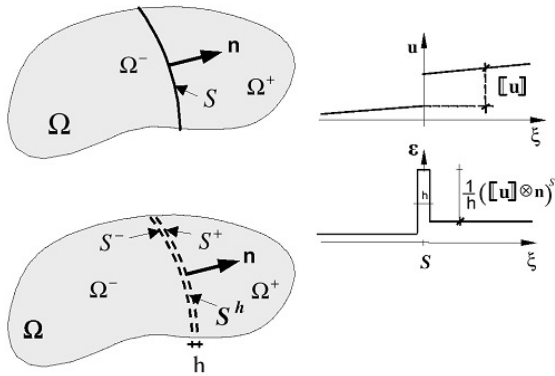


Figure 2: Kinematics of a discontinuity

### 2.2 Non-linear, dissipative, constitutive model equipped with strain softening

Among the large number of continuum constitutive models available for modeling of non-linear behavior and failure of concrete, the continuum damage models (Lemaitre (1985)) are becoming increasingly popular. Their simplicity, on one hand, and their ability to capture the secant stiffness degradation, experimentally observed in concrete in tensile states, on the other, makes them especially appealing. On this basis, and though there is no specific limitation in the CSDA on the selection of the constitutive model, we shall consider the following continuum damage model for failure of concrete:

$$\text{Free energy: } \begin{aligned} \Psi(\boldsymbol{\varepsilon}, r) &= (1-d)\psi_o \\ \Psi_o &= \frac{1}{2} \boldsymbol{\varepsilon} : \mathbf{C} : \boldsymbol{\varepsilon} \end{aligned} \quad (4)$$

$$\text{Damage variable: } d(r) = 1 - \frac{q(r)}{r} \quad (5)$$

$$\text{Internal variable: } \begin{aligned} \dot{r} &= \lambda \\ r|_{t=0} &= r_o = \sigma_u / \sqrt{E} \end{aligned} \quad (6)$$

$$\text{Constitutive law: } \begin{aligned} \boldsymbol{\sigma} &= \frac{\partial \Psi}{\partial \boldsymbol{\varepsilon}} = (1-d)\mathbf{C} : \boldsymbol{\varepsilon} \\ &= \frac{q}{r} \mathbf{C} : \boldsymbol{\varepsilon} = \frac{q}{r} \bar{\boldsymbol{\sigma}} \end{aligned} \quad (7)$$

$$\text{Damage function: } \begin{aligned} g(\boldsymbol{\varepsilon}, r) &\equiv \tau_\varepsilon(\boldsymbol{\varepsilon}) - r \\ \tau_\varepsilon(\boldsymbol{\varepsilon}) &\equiv \sqrt{\boldsymbol{\sigma}^+ \cdot \mathbf{C}^{-1} \cdot \boldsymbol{\sigma}} \end{aligned} \quad (8)$$

$$\text{Loading conditions: } \lambda \geq 0 \quad g \leq 0 \quad \lambda g = 0 \quad (9)$$

$$\text{Softening law: } \begin{aligned} \dot{q} &= H(r)\dot{r} \\ H &:= \begin{cases} H_0 = \text{constant} \\ \text{linear softening} \\ H_0 \exp\left(\frac{-r_0}{G_f}(r - r_o)\right) \\ \text{exponential softening} \end{cases} \end{aligned} \quad (10)$$

$$\dot{\boldsymbol{\sigma}} = \mathbf{C}^{\text{tan}} : \dot{\boldsymbol{\varepsilon}}$$

Incremental constitutive law:

$$\mathbf{C}^{\text{tan}} = \begin{cases} (1-d)\mathbf{C} = \frac{q}{r}\mathbf{C} & \text{unloading} \\ \frac{q}{r}\mathbf{C} - \frac{q-Hr}{r^3}\bar{\boldsymbol{\sigma}} \otimes \bar{\boldsymbol{\sigma}}^+ & \text{loading} \end{cases} \quad (11)$$

where  $d \in [0,1]$  is the damage variable,  $\Psi(\boldsymbol{\varepsilon}, r)$  is the free energy, depending on the strain tensor  $\boldsymbol{\varepsilon}$  and the internal variable  $r$ , and  $\psi_o$  is the elastic strain energy for the undamaged material;  $\mathbf{C} = \bar{\lambda}(\mathbf{1} \otimes \mathbf{1}) + 2\mu\mathbf{I}$  is the elastic constitutive tensor,  $\bar{\lambda}$  and  $\mu$  are the Lamé's parameters and  $\mathbf{1}$  and  $\mathbf{I}$  are the identity tensors of 2nd and 4th order, respectively.

In equation (7),  $\bar{\boldsymbol{\sigma}} = \mathbf{C} : \boldsymbol{\varepsilon}$  is the effective stress. Its positive counterpart is then defined as:

$$\bar{\boldsymbol{\sigma}}^+ = \langle \bar{\sigma}_i \rangle \mathbf{p}_i \otimes \mathbf{p}_i \quad (12)$$

where  $\langle \bar{\sigma}_i \rangle$  stands for the positive part (Mac Auley brackets) of the  $i$ -th principal effective stress  $\bar{\sigma}_i$  ( $\langle \bar{\sigma}_i \rangle = \bar{\sigma}_i$  for  $\bar{\sigma}_i \geq 0$  and  $\langle \bar{\sigma}_i \rangle = 0$  for  $\bar{\sigma}_i < 0$ ) and  $\mathbf{p}_i$  stands for the  $i$ -th principal stress eigenvector. The initial elastic domain defined as  $E_\sigma^0 := \{\boldsymbol{\sigma} ; \sqrt{\boldsymbol{\sigma}^+ \cdot \mathbf{C}^{-1} \cdot \boldsymbol{\sigma}} < r_o\}$  is then unbounded for compressive stress states ( $\boldsymbol{\sigma}^+ = \mathbf{0}$ ) and, therefore, damage becomes only associated to tension as usual for modeling cracking in concrete.

The actual stresses  $\boldsymbol{\sigma}$  and the stress-like variable  $q$  are determined via the state equations (7) and (10). Equation (10) defines the softening law in terms of the *continuum softening parameter*  $H \leq 0$ . In equation (6),  $\sigma_u$  and  $E$  are, respectively, the tensile strength and the Young modulus. Finally, equation (11) is the resulting rate constitutive law in terms of the tangent constitutive operator  $\mathbf{C}^{\text{tan}}$ .

One of the most attractive features of the previous model is that the internal variable  $r$  in equation (6), and then the rest of the model, can be straightforwardly integrated in terms of the current strains as:

$$r(t) = \max_{s \in [0,t]} [r_0, \tau_\boldsymbol{\varepsilon}(\boldsymbol{\varepsilon}(s))] \quad (13)$$

this making the model inexpensive and robust and, therefore, suitable for computational purposes.

### 2.3 Softening modulus regularization

As the discontinuous displacement field (1) is activated, the unbounded strains in equation (2) develop inside  $S^h$ . Furthermore, the equilibrium condition imposes the tractions  $\boldsymbol{\mathcal{T}} = \boldsymbol{\sigma} \cdot \mathbf{n}$  to be continuous in the neighborhood of  $S^h$ . Since the strains and stresses are regular outside  $S^h$  that condition enforces *boundedness* of the traction vector  $\boldsymbol{\mathcal{T}} = \boldsymbol{\sigma} \cdot \mathbf{n}$ , and therefore of the whole stress tensor in  $S^h$  which, in consequence, has to be bounded in presence of unbounded strains. As it has been proven in Oliver (2000), a sufficient condition for this to happen is to redefine the character of the softening modulus  $H$  as follows:

$$\frac{1}{H} = \delta_s \frac{1}{\bar{H}} \quad (14)$$

where  $\bar{H}$  is termed the *intrinsic softening modulus*, which can be characterized as a material parameter in terms of the fracture energy  $G_f$  the ultimate tensile strength  $\sigma_u$  and the Young modulus  $E$ :

$$\bar{H} = \underbrace{-\frac{\sigma_u^2}{2EG_f}}_{\text{linear softening case}} \quad (15)$$

$$\bar{H} = \underbrace{-\frac{\sigma_u^2}{EG_f} \exp\left(\frac{-r_0}{G_f}(r - r_o)\right)}_{\text{exponential softening case}}$$

Equation (15) clearly links the CSDA with non-linear fracture mechanics via the classical concept of fracture energy. The regularized version of equation (14) reads, after insertion of equation (3):

$$H = h\bar{H} \quad (16)$$

which is the so called *softening modulus regularization condition* (Oliver (2000)).

### 2.4 Induced (continuum-degenerated) traction separation law

The introduction, in the continuum constitutive model described by equations (4) to (11), of the strong discontinuity kinematics (1)-(2) and the softening modulus regularization (16), leads to a crucial result in the CSDA. In fact, it can be shown, see Oliver (2000), that a discrete constitutive damage model relating the traction  $\boldsymbol{\mathcal{T}} = \boldsymbol{\sigma} \cdot \mathbf{n}$  and the displacement jump  $[[\mathbf{u}]]$  is automatically fulfilled at the failure (cracking) interface  $S$  i.e.:

$$\begin{aligned} \text{Free energy: } \varphi([\mathbf{u}], \alpha) &= (1 - \omega)\varphi_o \\ \varphi_o &= \frac{1}{2} [[\mathbf{u}], \mathbf{Q} \cdot [[\mathbf{u}]] \end{aligned} \quad (17)$$

$$\mathbf{Q} = \mathbf{n} \cdot \mathbf{C} \cdot \mathbf{n}$$

$$\text{Damage variable: } \omega(\alpha) = 1 - \frac{q(\alpha)}{\alpha} \quad (18)$$

$$\begin{aligned} \text{Internal variable: } \dot{\alpha} &= \bar{\lambda} \\ \alpha|_{t=0} &= 0 \end{aligned} \quad (19)$$

$$\text{Traction-separation law: } \mathcal{T} = \frac{\partial \varphi}{\partial [[\mathbf{u}]]} = (1 - \omega)\mathbf{Q} \cdot [[\mathbf{u}]] \quad (20)$$

$$\begin{aligned} \text{Damage function: } \bar{g}([\mathbf{u}], \alpha) &\equiv \tau_{[[\mathbf{u}]]}([\mathbf{u}]) - \alpha \\ \tau_{[[\mathbf{u}]]} &\equiv \sqrt{\bar{\mathcal{T}}^+ \cdot \mathbf{Q}^{-1} \cdot \bar{\mathcal{T}}} \end{aligned} \quad (21)$$

$$\text{Loading conditions: } \bar{\lambda} \geq 0 \quad \bar{g} \leq 0 \quad \bar{\lambda} \bar{g} = 0 \quad (22)$$

$$\text{Softening law: } \dot{q} = \bar{H}(\alpha) \dot{\alpha} \quad (23)$$

$$\begin{aligned} \text{Incremental constitutive law: } \dot{\mathcal{T}} &= \mathbf{Q}^{\text{tan}} : [[\mathbf{u}]] \\ \mathbf{Q}^{\text{tan}} &= \begin{cases} (1 - \omega)\mathbf{Q} = \frac{q}{\alpha}\mathbf{Q} & \text{unloading} \\ \frac{q}{\alpha}\mathbf{Q} - \frac{q - \bar{H}\alpha}{\alpha^3}\mathcal{T} \otimes \mathcal{T}^+ & \text{loading} \end{cases} \end{aligned} \quad (24)$$

where  $\omega$  is a *discrete damage variable* playing a similar role in the traction-separation law (20) than  $d$  in the continuum damage model of equations (4)-(11). It can be proven a one-to-one correspondence of variables appearing in the continuum and discrete models, as shown in Table 1.

$\varphi = \lim_{h \rightarrow 0} h\Psi$	$\begin{aligned} & ([[ \mathbf{u} ] ] \otimes \mathbf{n})^S = \\ & = \lim_{h \rightarrow 0} h\boldsymbol{\varepsilon} \end{aligned}$	$\mathcal{T} = \boldsymbol{\sigma} \cdot \mathbf{n}$
$\mathbf{Q} = \mathbf{n} \cdot \mathbf{C} \cdot \mathbf{n}$	$\alpha = \lim_{h \rightarrow 0} hr$	$H = h\bar{H}$

Table 1: Correspondence of variables in the continuum an degenerated discrete models

As it can be readily checked, the induced discrete model consists of not only the traction-separation law (20), but a complete degenerated constitutive model equipped with all the ingredients sketched in equations (17)-(24).

Moreover, that degeneration is a *projection* of the original constitutive model into the failure surface  $S$  and the resulting model inherits its properties; for instance, discrimination from tension to compression by equation (8) is implicitly fulfilled in the projected model via equation (21).

Most interesting, the projection procedure and properties are not specific of any parent continuum constitutive model. On the contrary, *any standard continuum dissipative model, with the only requirement of being equipped with strain softening, can be projected, via the CSDA in a consistent traction-separation law*. This constitutes the intended bridge between continuum and fracture mechanics.

For modeling and simulation purposes, it is important to emphasize that *the discrete constitutive model is not necessarily derived and implemented in practice*, but fulfilled from the continuum model and the aforementioned ingredients. This fact constitutes one of the most relevant benefits of the CSDA to be exploited for computational purposes: *the analysis is kept in the continuum format but the results are the same that would be obtained with the induced traction-separation law in a classical non-linear fracture mechanics setting*. Typical drawbacks in discrete models, as the classical ill conditioning produced by the dummy initial stiffness (Simone, 2003), are then automatically circumvented.

As for calibration and validation, the CSDA can be also exploited: the parent continuum constitutive model can be assessed from classical laboratory tests, which provide averaged continuum mechanical measures in terms of the stresses and strains. Thus, there is no need to make artificial translations of those measures into less measurable entities as tractions and crack separations. Once the continuum model is calibrated, it can be, if desired, degenerated into the discrete one via the CSDA.

### 3 REPRESENTATIVE SIMULATIONS

The numerical results presented in this section have been obtained using the general-purpose finite element code COMET (Cervera et al. (2001)) where the specific ingredients of the CSDA are implemented and run in a PC equipped with a Pentium 4 processor.

### 3.1 Double notched specimen in mixed mode of fracture

A double-notched concrete specimen undergoing a mixed mode fracture, experimentally tested by Nooru-Mohamed (1992), is analyzed. The specimen is a concrete block, of 200x200[mm] size and 50.[mm] of thickness, with two deep symmetrical notches as shown in Figure 3. It is fixed to the loading device on those sides where loading and displacement conditions are imposed. An initial horizontal load force  $P_h = 5$ .(kN) is applied, which remains constant along the complete experiment. In a second stage, the loading device imposes an incremental vertical displacement  $\delta_v$ . Plane stress assumptions have been done for the modeling. Material parameter values are:  $E=30$ .[Gpa],  $\nu = 0.2$ ,  $\sigma_u = 3$ .(MPa). In the spirit of the CSDA, the fracture energy  $G_f = 110$ .(N/m) has been considered the same for both fracture modes I and II.

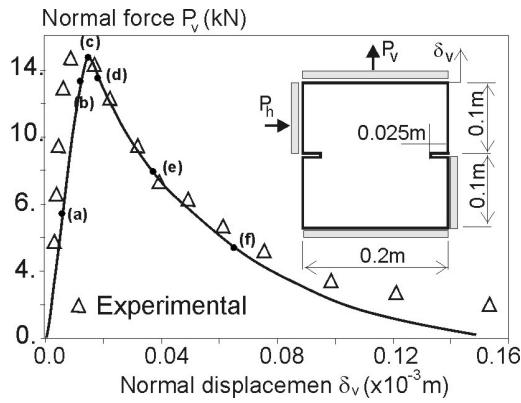


Figure 3: Double-notched specimen. Up: experimental test. Down: force versus vs. displacement curve.

The finite element mesh is made of 1572 quadrilateral elements including the rigid support, which has also been modeled.

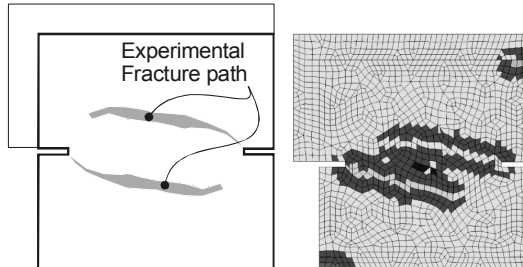


Figure 4: Double-notched specimen. Left: experimental crack pattern. Right: model crack pattern.

Figure 3 shows the vertical force versus the vertical displacement for both the numerical simulation and the experiment. It can be observed that numerical results provide a slight underestimation of the initial stiffness, but the peak load and the post-peak curve agree very well with the experimental test. In Figure 4 the numerical obtained crack patterns and the experimental ones display an excellent agreement.

Figure 5 presents the evolution of the modeled crack pattern obtained at the different stages of the deformation process marked in Figure 3 (the propagation direction was considered orthogonal to the first tensile principal stress). It can be observed that the upper main crack arrests at the peak load (point c) whereas the lower crack remains active.

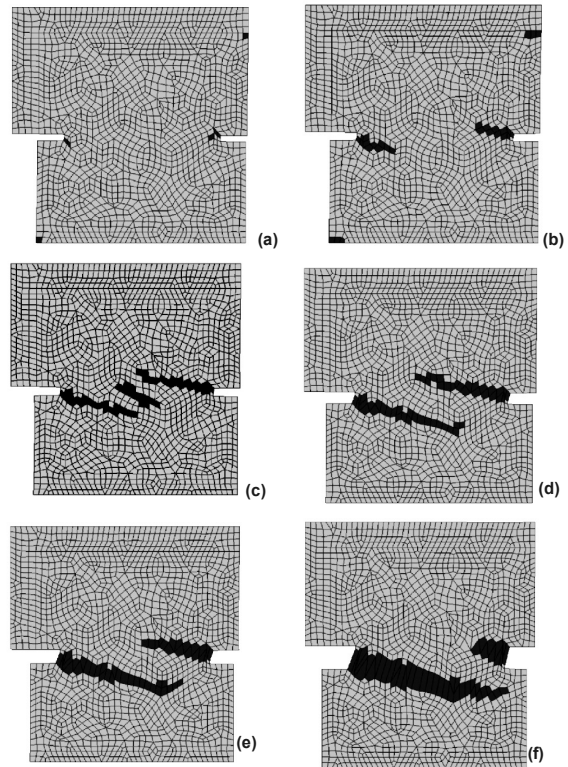


Figure 5: Double-notched specimen: active crack patterns displayed on the deformed specimen (amplification factor 100)

### 3.2 Pull out of a rebar in a concrete specimen

The goal of the test is to reproduce qualitatively the sequential process of formation of cracks, in reinforced concrete, due to the bond-slip effects in the concrete-steel interface. It is not intended to make an exhaustive study but to check if the proposed methodology could capture the essentials of cracking generation phenomena.

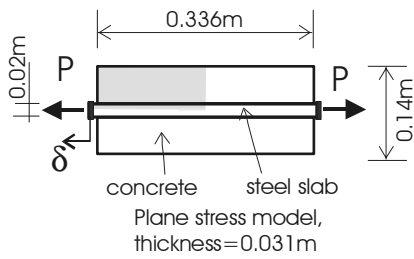


Figure 6: Pull out test

In the model a reinforced concrete specimen is subjected, under plane strain conditions, to the rebar pull out as shown in Figure 6 (in Rots (1988) a numerical solution of a similar configuration, assuming axial symmetry can be found). Adhesion along the steel–concrete interface is modeled using bond-slip elements with a rigid-perfectly plastic  $J_2$  (Von-Mises) material model.

Material	Model	E	$\nu$	$G_f$	$\sigma_u$
Concrete	Only traction damage	25.GPa	0.18	25 N/m	2.8 MPa
Reinforcement	Elastic	214. GPa	0.3	--	--
Joint	Rigid-Plastic ( $J_2$ )	----	0.3	--	3.0 MPa

Table 2: Material properties.

Due to the problem symmetries, only one fourth of the specimen was discretized. Additional material parameters characterizing the problem, Young's modulus,  $E$ , Poisson's ratio,  $\nu$ , ultimate tensile strength,  $\sigma_u$ , and fracture energy,  $G_f$  of concrete, as well as steel parameters and the sliding stress,  $\sigma_{yd}$ , of the bounding material are displayed in Table 2.

Results in Figure 7 and Figure 8, although not experimentally assessed, display the phenomena of crack development in reinforced concrete structures i.e.: in a first stage of the loading process a secondary crack system develops without causing substantial loss of the structural strength. Then, the loading increase leads to the formation of a first primary crack, propagating across the concrete section, producing a sudden loss of the strength of that concrete section marked by the sharp snap-back in the force-displacement curve of Figure 8.

Then, steel-concrete bond effects transfer the load to other sections of concrete leading to the formation of subsequent primary cracks.

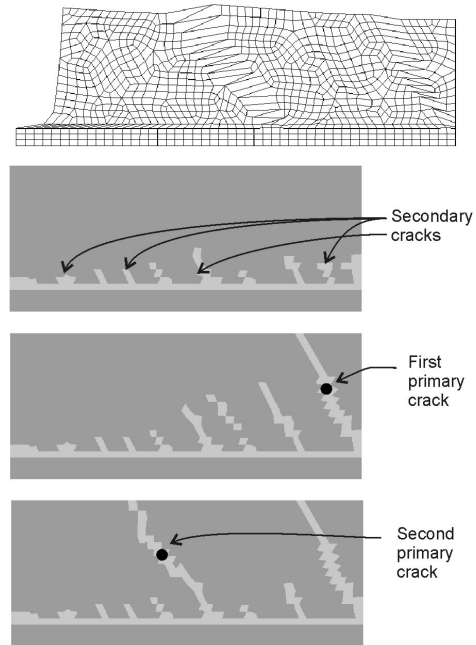


Figure 7: Pull out test: Deformed (amplified) finite element mesh and crack pattern evolution.

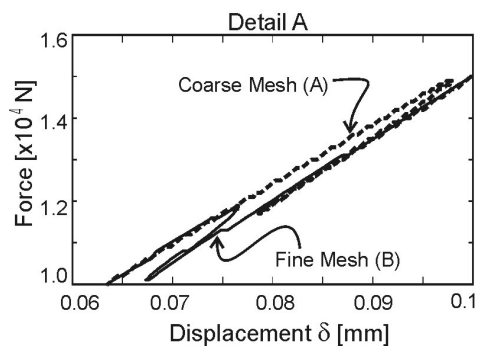
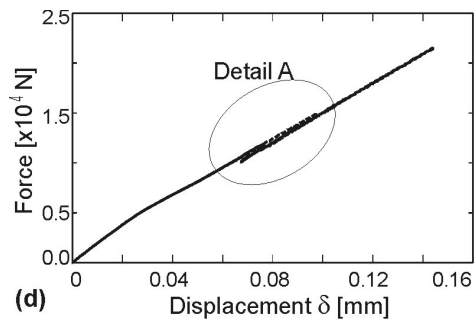


Figure 8: Pull out test. Force vs. displacement curve an detail of the structural snap-back

### 3.3 3D simulation of a four point shear test on a double notched beam

This test was reported in Bocca, Carpinteri & Valente (1990). In order to test the ability of the approach to reproduce multidimensional fracture problems, a 3D simulation has been performed using a relatively coarse finite element mesh (2967 tetrahedra). In Figure 9 the geometrical details of the test are presented. The authors of the experiment report the appearance of two cracks, starting from the two notches, as shown in the figure.

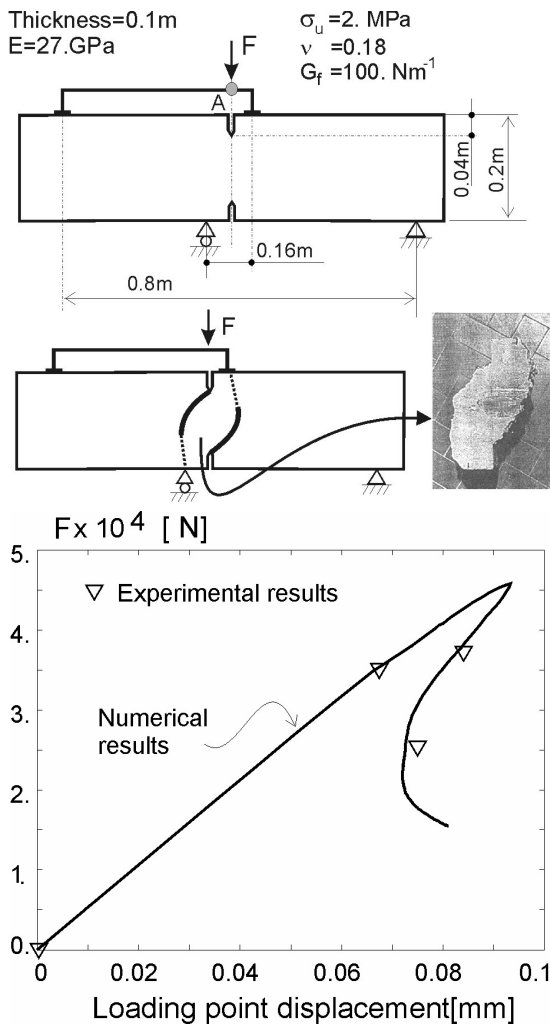


Figure 9: Four-point shear test. Experiment description and loading vs. displacement curve.

Those cracks are effectively reproduced in the numerical simulation as shown in Figure 10. Along the raising branch of the force-displacement curve, both cracks are active. At the peak, a bifurcation

process results in arresting of the right-hand crack, keeping the other active, and producing the final failure mode displayed in Figure 10.

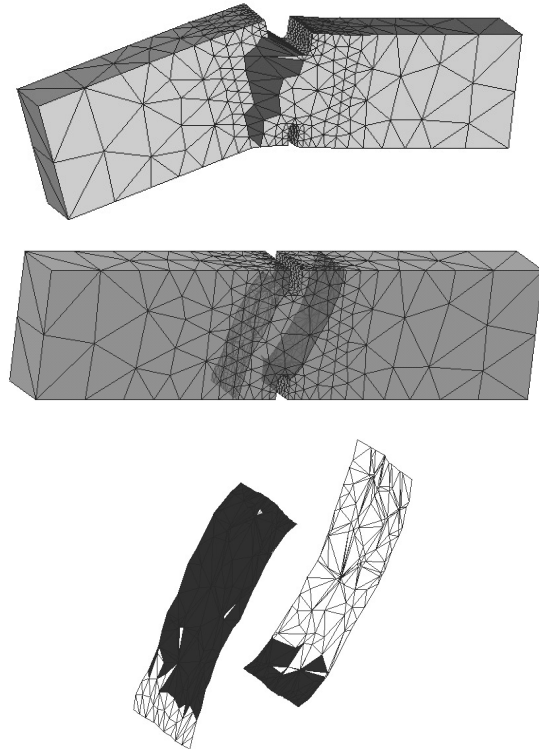


Figure 10: Four-point shear test. Up: failure mode (amplified). Middle: fracture surfaces. Down: detail of the fracture surfaces (cracked elemental surfaces displayed in dark).

## 4 CONCLUSIONS

The strong discontinuity approach has revealed as an appealing tool for modeling fracture phenomena in solids and, in particular, in concrete. In the preceding sections a specific branch, the so-called Continuum Strong Discontinuity Approach (CSDA), has been applied to the numerical simulation of fracture of concrete. In the light of those results, the following conclusions can be stated:

- The CSDA provides a clear connection of Continuum Mechanics with non-linear Fracture Mechanics. In fact, the introduction of the strong discontinuity kinematics and the softening modulus regularization, into a continuum constitutive model, induces the

fulfillment, at the discontinuity surface, of a traction-separation law that is as degeneration (projection onto the crack) of that model. Since the degenerated model has not necessarily to be explicitly derived and effectively implemented, this fact can be exploited for modeling both the continuum and fracture regimes of the deformation processes including the transition from each other (fracture process zone). In addition, that feature can be also exploited for identification of the fracture material properties in terms of continuum-like measures extracted from laboratory experiments.

- As for the modeling of the concrete fracture, the approach appears very appealing since a) it provides good representations of the complex phenomena of cracking b) accounts for multiple fractures developing simultaneously and interacting with each other, and c) does not require “a priori” determination of the crack paths.
- Numerical simulation in the context of the CSDA is inexpensive as compared with other approaches. Indeed, 3D simulations, of simple tests as the ones presented in this work displaying multiple fractures, can be done in personal computers in short times (minutes). The quantitative accuracy of the results is also remarkable.

## 5 ACKNOWLEDGMENTS

Financial support from the Spanish Ministry of Science and Technology, through grant MAT2001-3863-C03-03, and from the Catalan Government Research Department, through the CIRIT grant 2001-SGR 00262, is gratefully acknowledged.

## 6 REFERENCES

- Bazant Z.P. & Planas 1997, Fracture and size effect in concrete and other quasibrittle materials. CRC Press.
- Bocca P., Carpinteri A Valente S..1990. Size effects in the mixed mode crack propagation: softening and snap-back analysis. *Engineering Fracture Mechanics* (35)159-170
- Cervera M., Agelet de Saracibar C., Chiumenti M., 2001, *COMET: a multipurpose finite element code for numerical analysis in solid mechanics*. Technical University of Catalonia (UPC), Baercelona Spain
- Nooru-Mohamed N.B.1992. *Mixed mode fracture of concrete: an experimental approach*. Ph.D. Thesis, Delft University of Technology, Delft, Netherlands.
- Lemaitre J. 1985. A continuous damage mechanics model for ductile fracture. *J. of Engineering Materials and Technology, Trans. ASME*, (107):.83-89.
- Oliver J., Cervera M., Manzoli O. 1999. *Strong discontinuities and continuum plasticity models: the strong discontinuity approach*, *International Journal of Plasticity* (15):319-351
- Oliver J., 2000. On the discrete constitutive models induced by strong discontinuity kinematics and continuum constitutive equations. *Int. J. Solids and Structures* (37):7207-7229
- Oliver J., Huespe A.E., Pulido M.D.G., Chaves E., 2001. From continuum mechanics to fracture mechanics: the strong discontinuity approach. *Engineering Fracture Mechanics* 69(2): 113-136
- Rots J.G., 1988 *Computational modeling of Concrete Fracture*, PhD Thesis, Delft University of Technology.
- Simone A. 2003 *Continuous-Discontinuous modeling of failure*. Ph.D. Thesis, Delft University of Technology, Delft, Netherlands.